Earth and Planetary Science Letters 299 (2010) 242–249

Contents lists available at ScienceDirect

Earth and Planetary Science Letters

journal homepage: www.elsevier.com/locate/epsl

Tempo and scale of late Paleocene and early Eocene carbon isotope cycles: Implications for the origin of hyperthermals

James C. Zachos [a,*], Heather McCarren [a], Brandon Murphy [a], Ursula Röhl [b], Thomas Westerhold [b]

[a] Earth and Planetary Sciences Dept., University of California, Santa Cruz, CA 95064, USA
[b] MARUM, Center for Marine Environmental Sciences, University of Bremen, Leobener Strasse, 28359 Bremen, Germany

ARTICLE INFO

Article history:
Received 30 March 2010
Received in revised form 2 September 2010
Accepted 3 September 2010
Available online 17 September 2010

Editor: P. DeMenocal

Keywords:
Paleocene
Eocene
PETM
carbon isotopes
carbon cycle
global warming

ABSTRACT

The upper Paleocene and lower Eocene are marked by several prominent (>1‰) carbon isotope ($\delta^{13}C$) excursions (CIE) that coincide with transient global warmings, or thermal maxima, including the Paleocene–Eocene Thermal Maximum (PETM). The CIE, which are recorded mainly in marine sedimentary sequences, have also been identified in continental sequences, occurred episodically, and yet appear to be paced or triggered by orbital forcing. To constrain the timing and scale of the CIE relative to long-term baseline variability, we have constructed a 4.52 million year (myr) long, high-resolution (~3 kyr) bulk sediment carbon isotope record spanning the lower Eocene to upper Paleocene (C25r–C24n) from a pelagic sediment section recovered at ODP Site 1262 in the southeast Atlantic. This section, which was orbitally-tuned utilizing high-resolution core log physical property and geochemical records, is the most stratigraphically complete upper Paleocene to lower Eocene sequence recovered to date. Time-series analysis of the carbon isotope record along with a high-resolution Fe intensity record obtained by XRF core scanner reveal cyclicity with variance concentrated primarily in the precession (21 kyr) and eccentricity bands (100 and 400-kyr) throughout the upper Paleocene–lower Eocene. In general, minima in $\delta^{13}C$ correspond with peaks in Fe (i.e., carbonate dissolution), both of which appear to be in phase with maxima in eccentricity. This covariance is consistent with excess oceanic uptake of isotopically depleted carbon resulting in lower carbonate saturation during periods of high eccentricity. This relationship includes all late Paleocene and early Eocene CIE confirming pacing by orbital forcing. The lone exception is the PETM, which appears to be out of phase with the 400-kyr cycle, though possibly in phase with the 100-kyr cycle, reinforcing the notion that a mechanism other than orbital forcing and/or an additional source of carbon is required to account for the occurrence and unusual scale of this event.

1. Introduction

The early Cenozoic is characterized by a series of short-lived hyperthermals, or transient episodes of warming. The largest of the hyperthermals, the Paleocene Eocene Thermal Maximum (PETM or ETM-1) at roughly ~56 Mya, is marked by a global warming of >5 °C (Kennett and Stott, 1991; Sluijs et al., 2006; Thomas and Shackleton, 1996; Tripati and Elderfield, 2005), and was followed by at least two additional, but smaller warming events, ETM-2 and ETM-3, also known as the "ELMO", and "X" events, respectively (Agnini et al., 2009; Lourens et al., 2005; Zachos et al., 2004). All three hyperthermals are characterized by carbonate dissolution horizons and negative carbon isotope excursions (CIE) (Lourens et al., 2005; Nicolo et al., 2007; Stap et al., 2009; Thomas et al., 1999; Zachos et al., 2005), phenomena that can only be explained by the rapid (~<10^4) introduction of a large mass of isotopically depleted carbon, likely in excess of several hundred or thousand petagrams, to the ocean–atmosphere system (Dickens et al., 1997).

The exact trigger for the PETM remains a matter of controversy. Suggested sources of this carbon include the dissociation of methane hydrate deposits (Dickens et al., 1995), flood basalt volcanism and thermal combustion of organic matter (Storey et al., 2007; Svensen et al., 2004), and oxidation of soil or marine organic carbon (Higgins and Schrag, 2006; Kurtz et al., 2003). The hyperthermals and CIEs in turn are superimposed on longer secular trends in global climate and the mean $\delta^{13}C$ of the oceans (Nicolo et al., 2007; Stott et al., 1990; Zachos et al., 2001). Whatever the source, a key consideration is whether the PETM shares a similar origin as subsequent hyperthermals. One suggestion, for example, is that these events are genetically related, being triggered by orbital forcing, possibly by extreme phases of earth eccentricity (Lourens et al., 2005).

Clearly an important step to understanding the origin of the hyperthermals is to place them in the proper temporal context of short and longer-term variations in climate and the carbon cycle. The

* Corresponding author.
E-mail address: jzachos@pmc.ucsc.edu (J.C. Zachos).

0012-821X/$ – see front matter © 2010 Elsevier B.V. All rights reserved.
doi:10.1016/j.epsl.2010.09.004

first attempt was based on the construction of a high-resolution (~10 kyr) global carbon isotope record by Cramer et al. (2003). This required splicing of individual upper Paleocene and lower Eocene isotope records from several deep-sea sites (ODP Sites 690 and 1051; DSDP Site 550 and 577; Fig. 1). This spliced or stacked global carbon isotope record revealed clear periodicity with cycle wavelengths close to those associated with orbital eccentricity. The record was then tuned to an artificially derived orbital target curve, and each of the late Paleocene and early Eocene carbon isotope minima associated with these cycles was labeled using an alpha-numeric scheme (A–K). This included two of the CIE associated with the hyperthermals, H and I, each characterized by double 100-kyr $\delta^{13}C$ minima (H1 and H2, I1 and I2), which correlate with ubiquitous carbonate dissolution horizons (Zachos et al., 2004). Although the total duration of the lower Eocene (and Chron 24r) and number of eccentricity cycles was underestimated because of undetected stratigraphic gaps and splicing errors (see Lourens et al., 2005; Westerhold et al., 2007), the stacked record demonstrated that the climate and carbon cycle variability of the upper Paleocene and lower Eocene were both being paced by orbital forcing, and these cycles could potentially be correlated using carbon isotopes records.

One of the key stratigraphic challenges of developing long and continuous, orbitally-tuned high-resolution records for the upper Paleocene and lower Eocene was effectively addressed with the successful recovery of undisturbed, multicored early Cenozoic pelagic section(s) from five sites on Walvis Ridge during ODP Leg 208 (Zachos et al., 2004). High-resolution shipboard core log physical properties data, including magnetic susceptibility and color reflectance, were used to characterize lithologic cycles down to the cm-scale. The cycle frequencies in the upper Paleocene and lower Eocene sections were found to be concentrated in bandwidths that match those of Milankovitch cycles, specifically precession and eccentricity. The cycle patterns were sufficiently distinct that individual precession cycles could be correlated between holes and even sites, thus enabling assembly of composite sections while providing an internal chronometer for establishing sedimentation rates. Counting of the low frequency (i.e., eccentricity) cycles suggested that the composite sections were the stratigraphically most complete recovered to date for the Paleocene and lower Eocene with relatively uniform and high (11–15 m/m.y.) sedimentation rates (Lourens et al., 2005). Each section contained distinct dissolution horizons including those representing the PETM and hyperthermal ETM-2. Subsequently, an astronomical calibration of the upper Paleocene and lower Eocene sections was carried out by identifying the eccentricity (and precession) cycles as expressed in high-resolution XRF elemental data from 4 sites in the Leg 208 transect (Westerhold et al., 2007; Westerhold et al., 2008). The cycles, then tuned to the orbital eccentricity solutions of Laskar et al., (2004), indicated an orbital control on the hyperthermals.

In order to assess the relationship between orbital forcing, the carbon cycle and climate, including the hyperthermals, we generated a high-resolution 4.52 myr long bulk carbonate stable isotope ($\delta^{13}C$ and $\delta^{18}O$) time series spanning the P–E boundary at Site 1262. Together with XRF core-scanned Fe concentration data, and an orbitally-tuned age model (Westerhold et al., 2007), the records are evaluated using time-series analysis to identify periodicity and the relative phasing of cycles between records. We also compare our carbon isotope record with previously published records from pelagic cores to assess the integrity (e.g., completeness) of the existing global carbon isotope stratigraphy. In addition to providing the most continuous orbitally-tuned carbon isotope record for the late Paleocene and early Eocene, our results confirm that the larger amplitude oscillations and excursions in climate and the carbon cycle were entirely paced by orbital eccentricity with one possible exception, the PETM.

2. Site location and lithology

ODP Site 1262 is located on the northwestern flank of Walvis Ridge, a bathymetric high in the SE Atlantic that separates the Cape and Angola basins (Fig. 1). The paleodepth of this site at 56 Mya is estimated to have been ~3600 m (Zachos et al., 2004). The ridge is covered by a layer of interbedded carbonate oozes and chalks, and marls, the thickness of which decreases from 500 m at the top of the rise to 300 m at the basin floor in the vicinity of Site 1262 (Spieß et al., 2003). Cores were taken in 3 laterally offset holes (A, B, and C) at Site 1262 resulting in the successful recovery of a complete section (Zachos et al., 2004). The ~150 m thick upper Paleocene through lower Eocene sequence is comprised of clayey nannofossil ooze marked by sharp transitions to clay-rich facies coincident with ETM 1, 2, and 3. The composite splice and depth scale were assembled using magnetic susceptibility (MS) and sediment lightness (L^*) data from all 3 holes. Cores that experienced deformation or disturbance during the coring process were excluded from the composite splice that spans 0 to 236 mcd.

3. Methods

3.1. Fe and isotope analyses

Iron intensity (Fe) data for ODP Site 1262 were obtained at the MARUM, University of Bremen using an X-ray fluorescence (XRF) core scanner (Fig. 2) (Tjallingii et al., 2007; Westerhold et al., 2007). The XRF records are more consistent in terms of hole-to-hole agreement, and have a significantly higher signal-to-noise ratio than standard shipboard physical property measurements (Röhl and Abrams, 2000; Westerhold et al., 2007). As such, XRF data allow for the assembly of a

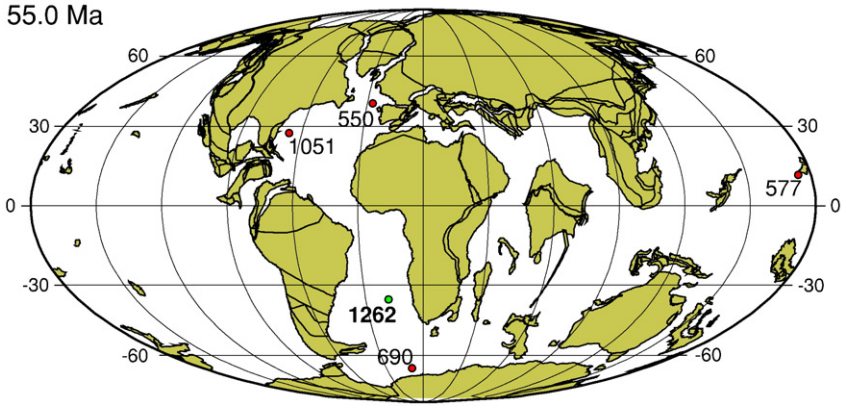

Fig. 1. Location map of ODP and DSDP sites considered in this study. The primary location for this study, ODP Site 1262, is located on Walvis Ridge.

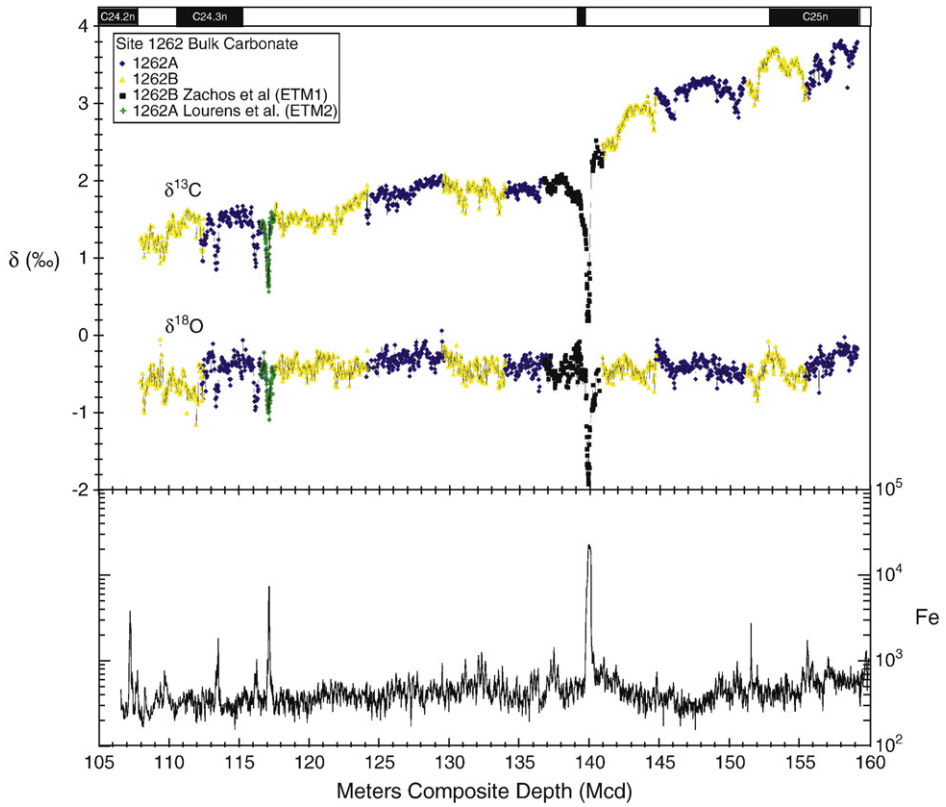

Fig. 2. Bulk sediment $\delta^{13}C$ and $\delta^{18}O$ (VPDB) and Fe records for ODP Site 1262 plotted versus meters composite depth (mcd; ~107.5 to 159.0). The isotope records are composites of the splice from the A and B holes of Site 1262, and include published data for the PETM and ETM-2 (Lourens et al., 2005; Zachos et al., 2005). Sampling resolution for the isotope records is ~3 cm with exception of the excursions (PETM and ETM-2) where the resolution is ~1 cm. The Fe intensity data, also a splice and plotted on a logarithmic scale, were obtained by high-resolution XRF core scanner (Westerhold et al., 2007). The C24 and C25 magnetochrons are plotted (Westerhold et al., 2007) along with a recently documented short normal within the PETM clay layer.
Lee and Kodama, 2009.

more accurate high-resolution composite depth scale (Röhl et al., 2000). Cores from the shipboard composite depth section (mcd) of Site 1262 were scanned every 2 cm over a 1 cm^2 area using 30 s count time. The sediments at this location are a mixture of two primary components, biogenic carbonate (i.e., foraminifer shells and coccoliths) and terrigenous clays (Zachos et al., 2004). As such, peaks in Fe intensity generally correlate to carbonate dissolution events, prominent examples being PETM and ETM-2, as the iron rich terrigenous clay fraction of total sediments increases in relative abundance.

Stable carbon and oxygen isotope analyses of crushed (freeze-dried) bulk sediment samples collected at a 1 to 3 cm interval from ~107 to 159 mcd (Fig. 2) were performed on an Autocarb coupled to either a PRISM or OPTIMA mass spectrometer at the UCSC Stable Isotope Laboratory. In both systems, samples are reacted in a common acid bath containing phosphoric acid at 90 °C and distilled in a single step. All values are reported relative to the VPDB standard. Analytical precision based on replicate analyses of in house standard Carrara Marble (n = 179) and NBS-19 (n = 16) averages 0.05‰ (1σ) for $\delta^{13}C$ and 0.09‰ (1σ) for $\delta^{18}O$.

3.2. Age model and time series analysis

The raw isotope records consist of 1806 data points (generated at ~1 to 3 cm intervals) spanning the interval ~107 to 159 mcd, and the Fe intensity record consists of 2072 data points spanning a slightly longer interval. The mcd were converted to age relative to the base of the CIE using a tuned age model (Westerhold et al., 2008). The tuning procedure was based on counting and alignment of eccentricity modulated precession (lithologic) cycles. Although the absolute age of the PETM is still floating because of uncertainties in radiometric dating and orbital solutions, multiple tuning options were identified that place the PETM somewhere within an 800 ky window (55.5 to 56.3 Ma) (Westerhold et al., 2008). For the purposes of this paper, however, absolute ages are unnecessary, so data are presented versus relative age (± m.y.) to the base of the PETM, or in the case of Site 1262, the base of the clay layer as represented by the peak in Fe (Fig. 3). Here we acknowledge that because of dissolution or chemical erosion, the base of the clay layer lies below the boundary within the upper Paleocene, and the actual onset of the CIE is located at least several cm higher within the clay layer.

In preparation for time-series analysis the isotope and Fe records were resampled at 2 ky intervals (originally ~3.5 and ~2.0 ky, respectively), and detrended using weighted (20%) means. The software package AnalySeries 2.0 (Paillard et al., 1996) was used to filter the time series for variability at periods of 400 kyr (0.025 ± 0.0005) and 100 kyr (0.01 ± 0.002). Prior to filtering, the PETM (ETM-1) excursion was removed from both the carbon isotope and Fe intensity time series in order to avoid skewing of cycles proximal to the CIE. Cross-spectral analysis for coherency and phase was carried out on the detrended carbon isotope (inverted) and Fe time series using the Arand software package (see Supporting online material), and evolutionary wavelet spectra obtained utilizing software provided by C. Torrence and G. Compo (http://paos.colorado.edu/research/wavelets).

4. Results

The 4.52 myr long bulk carbon isotope record is plotted versus depth in Fig. 2 and versus tuned age in Fig. 3. The record is characterized by a long-term decline of ~2.5‰. The decline is not smooth, but appears stepped, in part because of the low frequency $\delta^{13}C$ cycles and excursions

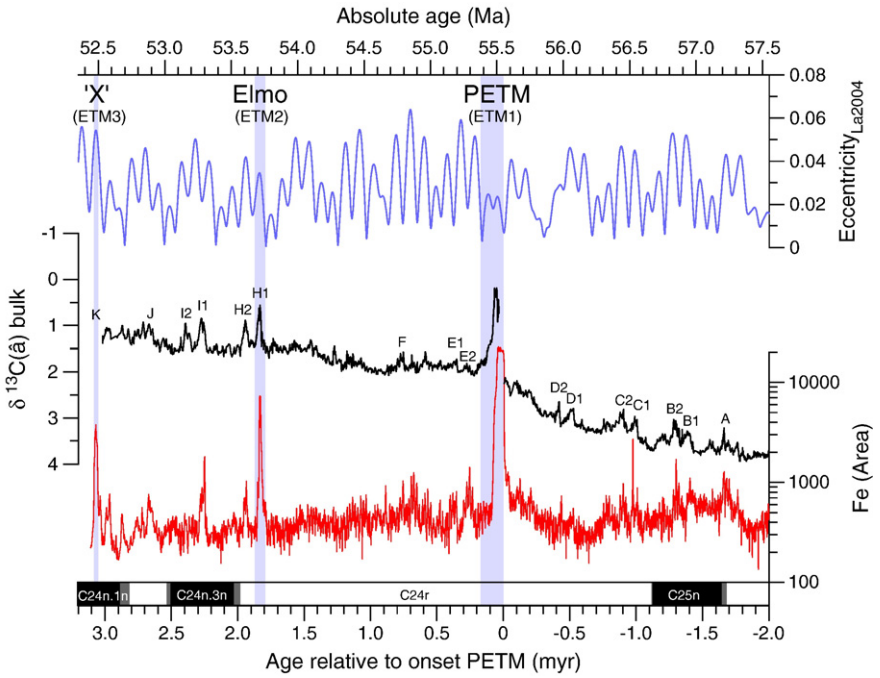

Fig. 3. The Site 1262 bulk sediment $\delta^{13}C$ isotope and Fe records plotted as ± millions of years (myr) relative to the base of the PETM (0.0 myr) on the lower axis. The $\delta^{13}C$ data and axis are inverted in this plot. The age model is based on tuning to the solution of eccentricity by Laskar et al. (2004). Although the astronomical solutions are undergoing further revision, we provide an absolute age model (upper axis) based on one of three tuning options, with an assigned age of 55.53 for the one based from the PETM (Westerhold et al., 2008). The other options are offset by roughly 400, and 800 k.y. In all 3 options the PETM is out of phase with the preceding 400 k.y. carbon isotope cycles and orbits, occurring in a minimum rather than a maximum with each option. The carbon cycle designations (A–K) of Cramer et al. (2003) are also included.

including the abrupt shift associated with the PETM. The low frequency cycles have wavelengths of roughly ~1 and 4 m, or 100 to 400 kyr, and amplitudes on the order of several tenths per mil. Higher frequency cycles have wavelengths of ~20 to 30 cm, or 21 kyr. Several carbon isotope excursions are clearly present in this record. The ETM-2 occurs at +1.83 Myr relative to PETM and is followed by a smaller excursion at +1.93 Myr. This pair, which is the equivalent of H1 and 2 of Cramer et al. (2003), is followed by another, but smaller pair of excursions roughly 400 kyr later, the equivalent of I1 and 2. Similar, but less pronounced paired excursions spaced at 400 kyr intervals are present in the upper Paleocene, and likely correlate with events A–D. Oscillations in the record of Fe intensity also vary at frequencies associated with the 100-kyr and 400-kyr cycles (Fig. 4B). As with the PETM, each of the CIE is coincident with a transient increase in Fe (i.e., or decrease in carbonate content), the magnitude of which generally scales with the magnitude of the CIE.

Wavelet and cross-spectral analysis of the bulk carbonate $\delta^{13}C_{carb}$ and Fe intensity records show a concentration of variance at frequencies corresponding to the long 400-kyr (0.0025) and short eccentricity 100-kyr (0.01), as well as precessional components at 23-kyr (0.0434) and 19-kyr (0.0526) (Figs. 4 and S1). The $\delta^{13}C$ and Fe records are highly coherent in the eccentricity bands, both 400 and 100 kyr, with maxima in Fe slightly leading minima in $\delta^{13}C$ by 10 to 20 kyr, respectively (Fig. S1). The records are also coherent in the precession band, although with $\delta^{13}C$ leading Fe (Fig. S1). Power in the obliquity band is present but relatively weak in both records, a common feature of Paleocene pelagic records (see Herbert and Dhondt, 1990; Westerhold and Rohl, 2009). The amplitude of the 100 and 400-kyr $\delta^{13}C$ cycles is pronounced (±0.2‰) over most of the record, but subdued in the interval (+1.0 Myr) immediately following PETM (Fig. 5). In contrast, the 400-kyr cycle amplitude in Fe, which is relatively subdued compared to the 100-kyr cycle amplitude, remains relatively constant over the entire transition.

The bulk carbonate $\delta^{18}O$ record is also plotted in Fig. 2. Over the long-term, the $\delta^{18}O$ record is stable, but over the short-term, $\delta^{18}O$ co-varies with $\delta^{13}C$, with variance concentrated in precession and eccentricity bands, and no discernible phase offsets. We limit further discussion of the oxygen isotope record for two reasons. The first is that bulk oxygen isotope values in carbonate rich sediments which have not been deeply buried, such as at Site 1262, are typically altered by early carbonate diagenesis (i.e., recrystallization) which occurs at low temperatures of bottom waters. While this process has negligible effects on carbon isotopes or the short-term trends in bulk carbonate $\delta^{18}O$, it can shift the overall mean value of $\delta^{18}O$ significantly (Schrag et al., 1995). Second, even with corrections, in the absence of large ice-sheets, the bulk $\delta^{18}O$ record must be recording largely a local temperature signal of some unconstrained part of the water column.

5. Discussion

5.1. Marine carbon isotope stratigraphy

The Site 1262 $\delta^{13}C_{carb}$ record is the longest high-resolution isotope record generated for the upper Paleocene–lower Eocene at a single location. Given the astronomical constraints on sedimentation rates and lack of evidence for any significant stratigraphic breaks, the Site 1262 record could serve as a standard reference section, the astronomical chronology of which could be transferred to other marine sections by correlation using high-resolution isotope stratigraphy. To begin the process of assessing the stratigraphic continuity of this record, as well as the nature of the long and short-term patterns, we compared the Site 1262 $\delta^{13}C_{carb}$ time series with the orbitally-tuned global stack or splice of Cramer et al. (2003), and the 4 records used to construct the stack (from DSDP Sites 550 and 577, and ODP Sites 690 and 1051; Fig. 6). The stack records were aligned side by side with 1262 using the base of PETM CIE as time zero. Lines of correlation were then drawn between equivalent $\delta^{13}C_{carb}$ minima in the 400-kyr cycles (cycles A–K of Cramer et al., 2003) as constrained by magnetostratigraphy, primarily the upper and lower boundaries of C24R (Westerhold et al., 2009). Aside from the CIE, the most robust correlation is over the upper and lower portions of these sections where the $\delta^{13}C$ cycles are most distinct, and also near the lower and

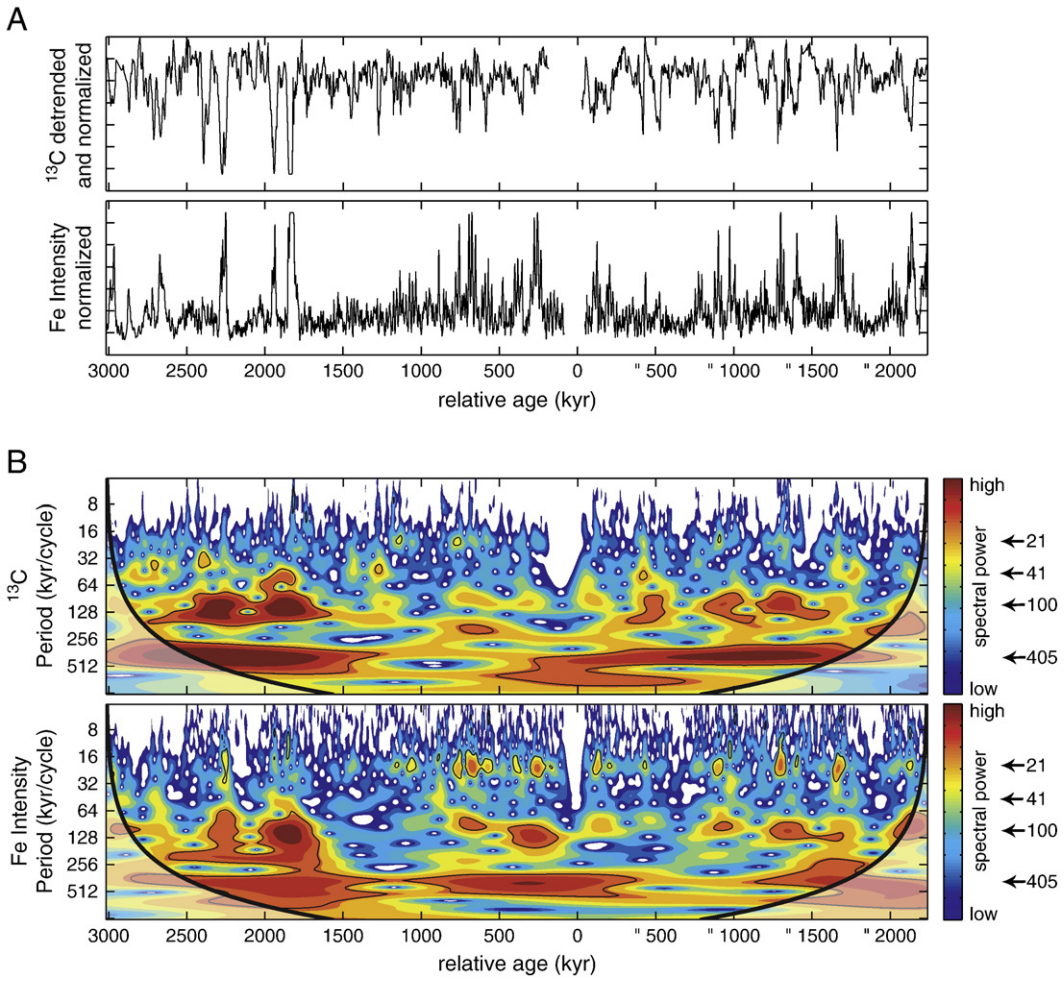

Fig. 4. (A) Detrended ODP Site 1262 $\delta^{13}C$ and Fe intensity data, and (B) and evolutionary wavelet power spectra plotted versus time (myr) relative to the onset of the PETM. The shaded contours in the evolutionary wavelet power spectra are normalized linear variances with blue representing low spectral power, and red representing high spectral power. The black contour lines enclose regions with more than 95% confidence. Shaded regions on either end indicate the cone of influence where edge effects become important. (Wavelet software by C. Torrence and G. Compo; http://paos.colorado.edu/research/wavelets).

upper boundaries of Chron 24R. From this comparison it is evident that the global stack underestimates the duration of time spanning the P–E boundary (between D2 and H1) by nearly 600 kyr, an error that likely stems from either miscorrelation or an undetected stratigraphic gap(s) in one or more of the DSDP and ODP sites used to construct the stack (see Lourens et al., 2005; Nicolo et al., 2007; Westerhold et al., 2007; Westerhold et al., 2009). Most of the missing record is located between PETM and H1, which is also the interval over which the eccentricity related $\delta^{13}C$ cycle amplitude is low, a factor that might have contributed to the previous misalignment of sections over this interval. A second gap in the splice must lie in the uppermost Paleocene portion of the stack (between PETM and D2), and is likely a consequence of an unconformity at Site 1051. This undetected gap likely contributed to the claim by Cramer et al. (2003) that the PETM lies only 7–9 (precession) cycles above D2, and thus could not have occurred during an eccentricity maximum. The one caveat for Site 1262 is the extensive chemical erosion of the PETM, a process which condensed roughly 20 to 40 kyr of the uppermost Paleocene into the clay layer (Zeebe and Zachos, 2007).

Correlation issues notwithstanding, it is clear that the long-term patterns and low frequency cycles in the Site 1262 bulk carbon isotope record are global in scale. The secondary Eocene CIE, H (1 and 2) and I (1 and 2), which occur in all high-resolution records that span those intervals, were paced by eccentricity, as were the late Paleocene carbon isotope minima, A through D. The PETM, though condensed at 1262, spans two 100-kyr eccentricity maxima suggesting that the signal of the second minima was either damped and/or swamped by the unusually large magnitude of the CIE, or simply that it occurred during a low amplitude phase of eccentricity. As already shown in several previous studies the low frequency Fe peaks, and by association minima in $\delta^{13}C_{carb}$, in the late Paleocene (A–C) and early Eocene (H–J) were likely in phase with maxima in the 400-kyr eccentricity cycle. The one exception is the PETM CIE, which was roughly ¼ cycle out of phase with the 400-ky maxima (Fig. 3). While it is possible this offset is an artifact of missing section below the boundary, and/or an error in the orbital tuning, possibly over an interval where the cycle amplitude is low (i.e., post-PETM), according to Westerhold et al. (2009) the estimated error in the Fe records and counts of precession cycles in the tuned model is two precession cycles at most. The implication is that the CIE was not the product of orbital forcing alone.

5.2. Speculation on the origin of carbon cycle oscillations

The prominent rise and fall of marine $\delta^{13}C$ over the late Paleocene and early Eocene (60–53 Mya) is a well known feature of all marine sections (Corfield and Norris, 1996; Shackleton, 1986; Zachos et al., 2001). Numerical modeling studies show that this trend could have been driven by changes in the flux of organic carbon to sediment reservoirs, most likely continental as indicated by sulfur isotopes (Kurtz

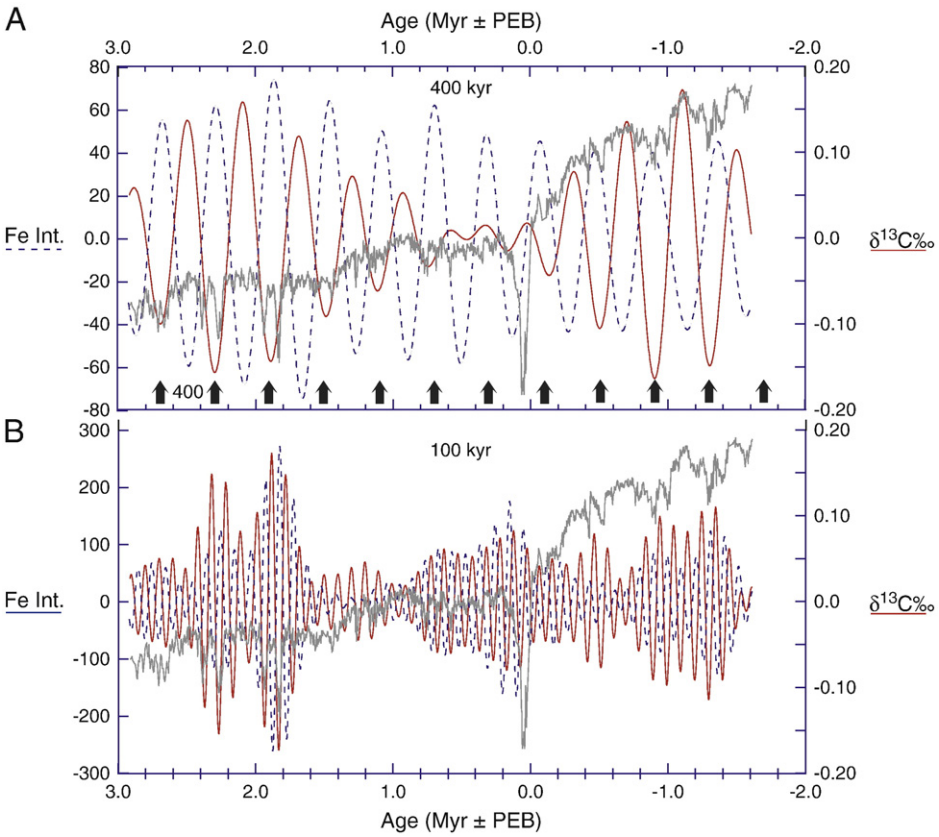

Fig. 5. (A) Low frequency (400-kyr) band pass filters of the tuned $\delta^{13}C_{carb}$ and Fe records for Site 1262 plotted along with the bulk isotope record. Arrows are at a fixed 400-kyr interval starting with the first $\delta^{13}C_{carb}$ minima in the upper Paleocene. (B) Low frequency (100 kyr) band pass filters of the tuned $\delta^{13}C_{carb}$ and Fe records plotted along with the bulk isotope record spanning the boundary.

et al., 2003). The key contribution of the tuned Site 1262 record is the more detailed characterization of the higher frequency variability including the frequency and amplitude of both the cyclical oscillations and excursions, including the PETM, in the context of long and short-term background variability (Fig. 3). Moreover, the isotope and Fe records establish the coherence between carbonate dissolution and carbon isotope cycles, a robust indication that the cycles were being driven by uptake/release of ^{12}C enriched carbon by a relatively mobile reservoir of reduced carbon. This includes the smaller CIE (e.g., ETM2), which were clearly in phase with the low frequency eccentricity cycles.

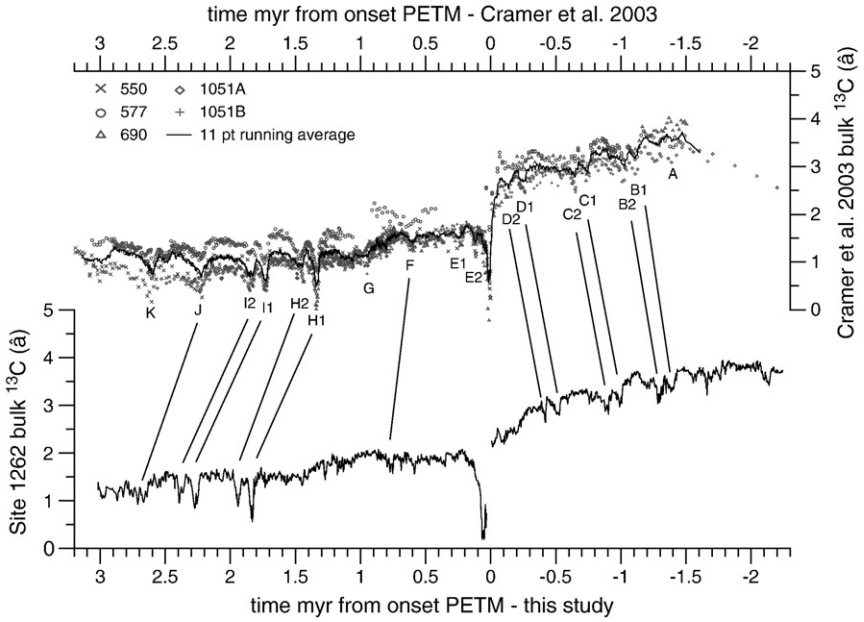

Fig. 6. The Site 1262 $\delta^{13}C$ time series plotted with the time series (DSDP and ODP Sites 550, 577, 690, and 1051) composing the global splice of Cramer et al. (2003). The tuned ages are relative to the PETM carbon isotope excursion. Lines of correlation between $\delta^{13}C$ minima (A–B and H–J) were constrained in part by their relation to magnetochron boundaries.

Volcanic related carbon emissions, either direct or indirect (i.e., combustion of crustal organics), though potentially capable of contributing to an excursion or two (e.g., Nisbet et al., 2009; Svensen et al., 2004), could not have been the primary driver of the periodic cycles.

How could the periodic expansion and decay of reduced carbon reservoirs have contributed to the prominent eccentricity dominated cycles in $\delta^{13}C$? To start, the $\delta^{13}C$ is highly coherent with the bulk $\delta^{18}O$, which coarsely represents relative changes in ocean temperature, and Fe, which represents changes in clay content and thus, the conditions that control carbonate preservation (i.e., local carbonate production and bottom water saturation). From this basic relationship, we can conclude that negative $\delta^{13}C$ excursions were driven by the release of isotopically depleted CO_2, which when absorbed by the ocean lead to undersaturation and dissolution of carbonate (i.e., higher Fe), as well as global warming. The opposite trends, that is rising $\delta^{13}C$, increased carbonate deposition, and global cooling, were all driven by the sequestration of isotopically depleted CO_2. As with the long-term trends, these patterns could easily be achieved by oscillating the transfer of relatively ^{12}C enriched carbon into a reduced carbon sediment reservoir, such as continental peats, marine sediments (i.e., shelf), or even methane hydrates.

The concentration of variance in the eccentricity and precession frequency bands is an important clue for indentifying the nature of coupling between forcing, climate, and the carbon cycle. Previous studies have documented similar periodicities in carbon isotope records of the Paleogene and the Late Cretaceous (Herbert, 1997; Herbert and Dhondt, 1990) as well as in the Oligocene and Miocene (Zachos et al., 2001). The oscillations in global $\delta^{13}C$ reflect shifts in the partitioning of carbon between ^{12}C depleted (oxidized) and ^{12}C enriched (reduced) carbon reservoirs. Modeling studies utilizing an ocean carbon cycle model with a simplified climate parameterization paced by orbital forcing, demonstrated how variance in the eccentricity bands during the Oligocene could be amplified by a resonance effect created by the long residence time of carbon in the ocean (~100 kyr) (Palike et al., 2006). While a similar resonance effect might have contributed to the pronounced eccentricity paced cyclicity of the Paleocene and Eocene, we offer an alternative, though not mutually exclusive, mechanism; that the primary coupling of orbital forcing, climate and the carbon cycle involved the accumulation of organic carbon not in the ocean, but on land.

Organic-rich peat was a significant carbon sink during the late Paleocene (Beerling, 2000; Kurtz et al., 2003) as is evident in the distribution of lignite and coal throughout North America and Eurasia (Duff, 1987; Ellis et al., 1999; Nagy, 2005; Ross and Ross, 1984). Some of the most massive coal sequences, such as those deposited in Wyoming, were produced within intermontane fluvio-deltaic systems bounding large lakes and/or interchannel areas of flood plains, as opposed to earl Paleocene and Cretaceous coals which were largely produced in coastal swamps (Warwick and Stanton, 1988). Peat deposition on such vast regional and global scales would suggest primarily a climatic control on wetland extent, specifically the seasonal distribution of precipitation, which in turn should be sensitive to eccentricity (Morrill et al., 2001; Valdes and Glover, 1999). Experiments with energy balance models have demonstrated how the climate effects of eccentricity are enhanced via its modulation of precession and thus differential land–sea heating and seasonal climate cycles in low latitudes (Crowley et al., 1992; Short et al., 1991). The seasonal land–sea heating, in turn, strongly influences precipitation patterns and intensity, particularly the monsoons. We posit that during eccentricity maxima, a shift to "monsoon-like" precipitation would lead to intense, but short wet seasons, and prolonged dry seasons, whereas during eccentricity minima, annual precipitation was seasonally more uniform. The latter should be more favorable for maintaining wetlands and accumulating peat, and thus increasing organic carbon burial. As eccentricity increased, a return to prolonged dry seasons would reverse the trend reducing the accumulation of organic carbon, while also promoting oxidation of existing peat (or lignite) through desiccation. The release of CO_2 would enhance warming, further amplifying seasonal extremes (Meehl et al., 2007), while also providing a potential positive feedback for fueling the hyperthermals (Kurtz et al., 2003; Wing et al., 2005). A strong orbital control on coal formation is supported in part by observations from the massive upper Paleocene coal seams of Wyoming, which show evidence of cyclic deposition with frequencies matching precession and eccentricity (Large et al., 2003). Moreover, evidence for increased erosion indicating enhanced seasonal extremes in precipitation during the PETM and subsequent hyperthermals has been documented in a number of locations (John et al., 2008; Nicolo et al., 2007; Schmitz and Pujalte, 2007).

Another potentially significant reduced carbon reservoir that might have driven or contributed to the high amplitude cyclicity in the carbon isotope record and climate as well as the CIE and hyperthermals is the methane hydrate reservoir. Marine sedimentary hydrates in particular could have been expanding and contracting in response to orbitally driven changes in climate (e.g., ocean temperature), sedimentation rates, and/or productivity, eventually completely discharging during the PETM. This so-called hydrate capacitor (Dickens, 2000; Dickens, 2003) would explain several features of the hyperthermals, including the anomalous and extreme magnitude of the PETM, in addition to the carbon isotope cycles. The partial or near complete discharge of the methane hydrate reservoir would also provide a means of driving the CIEs (Dickens, 2003), though subsequent recharging of this reservoir might require millions of years (Archer and Buffett, 2005). The latter might even explain the reduced magnitude of oscillations immediately following the event. Exactly how eccentricity would modulate the formation of marine hydrates, however, is not immediately obvious, though a coupling to climate via runoff or some other process seems plausible.

6. Summary

Our 4.52 myr long orbitally-tuned carbon isotope record for Site 1262 is the longest and most complete assembled to date for the late Paleocene and early Eocene, and thus provides a robust framework for evaluating and understanding the origin of carbon cycle excursions and related climate changes. It is evident that much of the short-term variability in the carbon cycle and climate during this interval was modulated by orbital forcing, specifically precession and eccentricity, both 100 and 400 kyr. This includes the secondary thermal maxima and carbon isotope excursions in the early Eocene, all of which likely are in phase with maxima in eccentricity. The PETM CIE, on the other hand, appears to have been out of phase with the long-term background (orbital) 400 k.y. cyclicity (Rohl et al., 2007). While some other component of orbital forcing might have triggered the PETM, either the 100 k.y. cycle, or even a low frequency component of orbital forcing (Galeotti et al., 2010), such a link is not evident in the Site 1262 record. For the moment, the out of phase relationship of the PETM and orbital forcing, along with the unusual magnitude of the event suggests that other processes must have triggered and/or amplified the PETM.

Acknowledgments

We thank Dyke Andreasen, Justin Yeakel, and Ryan Haupt for technical support, and Heiko Pälike, Jerry Dickens, Richard Zeebe, Luc Lourens, Lee Kump, and Appy Sluijs for contributions to key aspects of this work, as well as comments on drafts of the manuscript. Ellen Thomas and Claudia Agnini provided thoughtful reviews that significantly improved the manuscript. Sediment samples were supplied by the Ocean Drilling Program. This study was supported by NSF Grants EAR-0628719 and OCE-0903014 to J.Z. and by the Deutsche Forschungsgemeinschaft to U.R.

Appendix A. Supplementary data

Supplementary materials related to this article can be found online at doi:10.1016/j.epsl.2010.09.004.

References

Agnini, C., et al., 2009. An early Eocene carbon cycle perturbation at similar to 52.5 Ma in the Southern Alps: chronology and biotic response. Paleoceanography 24.

Archer, D., Buffett, B., 2005. Time-dependent response of the global ocean clathrate reservoir to climatic and anthropogenic forcing. Geochem. Geophys. Geosyst. 6.

Beerling, D.J., 2000. Increased terrestrial carbon storage across the Palaeocene–Eocene boundary. Palaeogeogr. Palaeoclimatol. Palaeoecol. 161 (3–4), 395–405.

Corfield, R.M., Norris, R.D., 1996. Deep water circulation in the Paleogene Ocean. In: Knox, R.W., Corfield, R.M., Dunay, R.E. (Eds.), Correlation of the Early Paleogene in Northwest Europe. : Geological Society Special Publication. Geological Society, London, pp. 443–456.

Cramer, B.S., Wright, J.D., Kent, D.V., Aubry, M.P., 2003. Orbital climate forcing of delta C-13 excursions in the late Paleocene-early Eocene (chrons C24n-C25n). Paleoceanography 18 (4).

Crowley, T.J., Kim, K.Y., Mengel, J.G., Short, D.A., 1992. Modeling 100, 000-year climate fluctuations in Pre-Pleistocene time-series. Science 255 (5045), 705–707.

Dickens, G.R., 2000. Methane oxidation during the Late Palaeocene Thermal Maximum. Bull. Soc. Geol. Fr. 171 (1), 37–49.

Dickens, G.R., 2003. Rethinking the global carbon cycle with a large, dynamic and microbially mediated gas hydrate capacitor. Earth Planet. Sci. Lett. 213 (3–4), 169–183.

Dickens, G.R., Oneil, J.R., Rea, D.K., Owen, R.M., 1995. Dissociation of oceanic methane hydrate as a cause of the carbon isotope excursion at the end of the Paleocene. Paleoceanography 10 (6), 965–971.

Dickens, G.R., Castillo, M.M., Walker, J.C.G., 1997. A blast of gas in the latest Paleocene: simulating first-order effects of massive dissociation of oceanic methane hydrate. Geology 25 (3), 259–262.

Duff, P.M.D., 1987. Mesozoic and Tertiary coals: a major world energy resource. Mod. Geology 11, 29–50.

Ellis, M.S., et al., 1999. Coal Resources. Powder River basin, USGS.

Galeotti, S., et al., 2010. Orbital chronology of early Eocene hyperthermals from the Contessa Road section, central Italy. Earth Planet. Sci. Lett. 290 (1–2), 192–200.

Herbert, T.D., 1997. A long marine history of carbon cycle modulation by orbital–climatic changes. Proc. Natl Acad. Sci. USA 94 (16), 8362–8369.

Herbert, T.D., Dhondt, S.L., 1990. Precessional climate cyclicity in late cretaceous early tertiary marine sediments — a high resolution chronometer of cretaceous tertiary boundary events. Earth Planet. Sci. Lett. 99 (3), 263–275.

Higgins, J.A., Schrag, D.P., 2006. Beyond methane: towards a theory for the Paleocene–Eocene Thermal Maximum. Earth Planet. Sci. Lett. 245 (3–4), 523–537.

John, C.M., et al., 2008. North American continental margin records of the Paleocene–Eocene thermal maximum: implications for global carbon and hydrological cycling. Paleoceanography 23 (2).

Kennett, J.P., Stott, L.D., 1991. Abrupt deep-sea warming, palaeoceanographic changes and benthic extinctions at the end of the Palaeocene. Nature 353 (6341), 225–229.

Kurtz, A., Kump, L.R., Arthur, M.A., Zachos, J.C., Paytan, A., 2003. Early Cenozoic decoupling of the global carbon and sulfur cycles. Paleoceanography 18, 1090.

Large, D.J., et al., 2003. High-resolution terrestrial record of orbital climate forcing in coal. Geology 31 (4), 303–306.

Laskar, J., et al., 2004. A long-term numerical solution for the insolation quantities of the Earth. Astronomy & Astrophysics 428 (1), 261–285.

Lee, Y.S., Kodama, K., 2009. A possible link between the geomagnetic field and catastrophic climate at the Paleocene–Eocene thermal maximum. Geology 37 (11), 1047–1050.

Lourens, L.J., et al., 2005. Astronomical pacing of late Palaeocene to early Eocene global warming events. Nature 435 (7045), 1083–1087.

Meehl, G.A., Stocker, T.F., Collins, W.D., Friedlingstein, P., Gaye, A.T., Gregory, J.M., Kitoh, A., Knutti, R., Murphy, J.M., Noda, A., Raper, S.C.B., Watterson, I.G., Weaver, A.J., Zhao, Z.-C., 2007. Global Climate Projections. In: Solomon, S., Qin, D., Manning, M., Chen, Z., Marquis, M., Averyt, K.B., Tignor, M., Miller, H.L. (Eds.), Climate Change 2007: The Physical Science Basis. : Contribution of Working Group I to the Fourth Assessment Report of the Intergovernmental Panel on Climate Change. Cambridge University Press, Cambridge.

Morrill, C., Small, E.E., Sloan, L.C., 2001. Modeling orbital forcing of lake level change: Lake Gosiute (Eocene), North America. Glob. Planet. Change 29 (1–2), 57–76.

Nagy, J., 2005. Delta-influenced foraminiferal facies and sequence stratigraphy of Paleocene deposits in Spitsbergen. Palaeogeogr. Palaeoclimatol. Palaeoecol. 222 (1–2), 161–179.

Nicolo, M.J., Dickens, G.R., Hollis, C.J., Zachos, J.C., 2007. Multiple early Eocene hyperthermals: their sedimentary expression on the New Zealand continental margin and in the deep sea. Geology 35 (8), 699–702.

Nisbet, E.G., et al., 2009. Kick-starting ancient warming. Nat. Geosci. 2 (3), 156–159.

Paillard, D., Labeyrie, L., Yiou, P., 1996. Macintosh program performs time-series analysis. EOS Trans. AGU 77, 379.

Palike, H., et al., 2006. The heartbeat of the Oligocene climate system. Science 314 (5807), 1894–1898.

Röhl, U., Abrams, L.J., 2000. High-resolution, downhole and non-destructive core measurements from Sites 999 and 1001 in the Caribbean Sea: application to the Late Paleocene Thermal Maximum, vol. 165. Ocean Drilling Program, College Station, TX.

Rohl, U., Westerhold, T., Bralower, T.J., Zachos, J.C., 2007. On the duration of the Paleocene–Eocene thermal maximum (PETM). Geochem. Geophys. Geosyst. 8.

Röhl, U., Bralower, T.J., Norris, R.D., Wefer, G., 2000. New chronology for the late Paleocene thermal maximum and its environmental implications. Geology 28 (10), 927–930.

Ross, C.A., Ross, J.R.P., 1984. Geology of Coal. John Wiley, Hoboken, N. J.. 349 pp.

Schmitz, B., Pujalte, V., 2007. Abrupt increase in seasonal extreme precipitation at the Paleocene–Eocene boundary. Geology 35 (3), 215–218.

Schrag, D.P., dePaolo, D.J., Richter, F.M., 1995. Reconstructing past sea surface temperatures: correcting for diagenesis of bulk marine carbonate. Geochem. Cosmochem. Acta 59, 2265–2278.

Shackleton, N.J., 1986. Paleogene stable isotope events. Palaeogeogr. Palaeoclimatol. Palaeoecol. 57 (1), 91–102.

Short, D.A., Mengel, J.G., Crowley, T.J., Hyde, W.T., North, G.R., 1991. Filtering of Milankovitch cycles by Earth's geography. Quatern. Res. 35 (2), 157–173.

Sluijs, A., et al., 2006. Subtropical Arctic Ocean temperatures during the Palaeocene/Eocene thermal maximum. Nature 441 (7093), 610–613.

Spieß, V., et al., 2003. Report and preliminary results of Meteor Cruise M49/1 Cape Town (South Africa)–Montevideo (Uruguay) 04.01.2000-10.02.2000. 205, Berichte, Fachbereich Geowissenschaften. Universitat Bremen, Bremen.

Stap, L., Sluijs, A., Thomas, E., Lourens, L., 2009. Patterns and magnitude of deep sea carbonate dissolution during Eocene Thermal Maximum 2 and H2, Walvis Ridge, Southeastern Atlantic Ocean. Paleoceanography 24.

Storey, M., Duncan, R.A., Swisher, C.C., 2007. Paleocene–Eocene thermal maximum and the opening of the northeast Atlantic. Science 316 (5824), 587–589.

Stott, L.D., Kennett, J.P., Shackleton, N.J., Corfield, R.M., 1990. The evolution of Antarctic surface waters during the Paleogene; inferences from the stable isotopic composition of planktonic foraminifers, ODP Leg 113. Proceedings of the Ocean Drilling Program, Weddell Sea, Antarctica, covering Leg, vol. 113, pp. 689–697.

Svensen, H., et al., 2004. Release of methane from a volcanic basin as a mechanism for initial Eocene global warming. Nature 429, 524–527.

Thomas, E., Shackleton, N.J., 1996. The Paleocene–Eocene benthic foraminiferal extinction and stable isotope anomalies. In: Knox, R.W.O.B., Corfield, R.M., Dunay, R.E. (Eds.), Correlation of the Early Paleogene in Northwest Europe. Geological Society Special Publication, London, pp. 401–441.

Thomas, D.J., Bralower, T.J., Zachos, J.C., 1999. New evidence for subtropical warming during the late Paleocene thermal maximum: stable isotopes from Deep Sea Drilling Project Site 527, Walvis Ridge. Paleoceanography 14 (5), 561–570.

Tjallingii, R., Rohl, U., Kolling, M., Bickert, T., 2007. Influence of the water content on X-ray fluorescence core-scanning measurements in soft marine sediments. Geochem. Geophys. Geosyst. 8.

Tripati, A., Elderfield, H., 2005. Deep-sea temperature and circulation changes at the Paleocene–Eocene thermal maximum. Science 308 (5730), 1894–1898.

Valdes, P.J., Glover, R.W., 1999. Modelling the climate response to orbital forcing. Philos. Trans. R. Soc. London Ser. A-Math. Phys. Eng. Sci. 357 (1757), 1873–1890.

Warwick, P.D., Stanton, R.W., 1988. Depositional models for 2 tertiary coal-bearing sequences in the Powder River Basin, Wyoming, USA. J. Geol. Soc. 145, 613–620.

Westerhold, T., Rohl, U., 2009. High-resolution cyclostratigraphy of the early Eocene — new insights into the origin of the Cenozoic cooling trend. Climate of the Past 5 (3), 309–327.

Westerhold, T., et al., 2007. On the duration of magnetochrons C24r and C25n and the timing of early Eocene global warming events: implications from the Ocean Drilling Program Leg 208 Walvis Ridge depth transect. Paleoceanography 22 (1).

Westerhold, T., et al., 2008. Astronomical calibration of the Paleocene time. Palaeogeogr. Palaeoclimatol. Palaeoecol. 257 (4), 377–403.

Westerhold, T., Rohl, U., McCarren, H.K., Zachos, J.C., 2009. Latest on the absolute age of the Paleocene–Eocene Thermal Maximum (PETM): new insights from exact stratigraphic position of key ash layers +19 and −17. Earth Planet. Sci. Lett. 287 (3–4), 412–419.

Wing, S.L., et al., 2005. Transient floral change and rapid global warming at the Paleocene–Eocene boundary. Science 310 (5750), 993–996.

Zachos, J., Pagani, M., Sloan, L., Thomas, E., Billups, K., 2001a. Trends, rhythms, and aberrations in global climate 65 Ma to present. Science 292 (5517), 686–693.

Zachos, J.C., Shackleton, N.J., Revenaugh, J.S., Palike, H., Flower, B.P., 2001b. Climate response to orbital forcing across the Oligocene–Miocene boundary. Science 292 (5515), 274–278.

Zachos, J.C., Kroon, D., Blum, P., 2004. Proc. ODP, Initial Reports, vol. 208. College Station. al., e.

Zachos, J.C., et al., 2005. Rapid acidification of the ocean during the Paleocene–Eocene thermal maximum. Science 308 (5728), 1611–1615.

Zeebe, R.E., Zachos, J.C., 2007. Reversed deep-sea carbonate ion basin gradient during Paleocene–Eocene thermal maximum. Paleoceanography 22 (3).